Aerosol Science and Technology

ISSN: (Print) (Online) Journal homepage: www.tandfonline.com/journals/uast20

Compact, high-flow, water-based, turbulent-mixing, condensation aerosol concentrator for collection of spot samples

Orthodoxia Zervaki, Dionysios D. Dionysiou & Pramod Kulkarni

To cite this article: Orthodoxia Zervaki, Dionysios D. Dionysiou & Pramod Kulkarni (2024) Compact, high-flow, water-based, turbulent-mixing, condensation aerosol concentrator for collection of spot samples, Aerosol Science and Technology, 58:8, 889-901, DOI: 10.1080/02786826.2024.2361050

To link to this article: https://doi.org/10.1080/02786826.2024.2361050

AEROSOL SCIENCE AND TECHNOLOGY
2024, VOL. 58, NO. 8, 889–901
https://doi.org/10.1080/02786826.2024.2361050

Compact, high-flow, water-based, turbulent-mixing, condensation aerosol concentrator for collection of spot samples

Orthodoxia Zervaki[a,b], Dionysios D. Dionysiou[b], and Pramod Kulkarni[a]

[a]Centers for Disease Control and Prevention, National Institute for Occupational Safety and Health, Cincinnati, Ohio, USA; [b]Environmental Engineering and Science Program, Department of Chemical and Environmental Engineering (ChEE), University of Cincinnati, Cincinnati, Ohio, USA

ABSTRACT

A new high-flow, compact aerosol concentrator, using rapid, turbulent mixing to grow aerosol particles into droplets for dry spot sample collection, has been designed and tested. The "TCAC (Turbulent-mixing, Condensation Aerosol Concentrator)" is composed of a saturator for generating hot vapor, a mixing section where the hot vapor mixes with the cold aerosol flow, a growth tube where condensational droplet growth primarily occurs, and a converging nozzle that focuses the droplets into a beam. The prototype concentrator utilizes an aerosol sample flow rate of 4 L min^{-1}. The TCAC was optimized by varying the operating conditions, such as relative humidity of the aerosol flow, mixing flow ratio, vapor temperature, and impaction characteristics. The results showed that particles with a diameter $\geq$ 25 nm can be grown to a droplet diameter $>$ 1400 nm with near 100% efficiency. Complete activation and growth were observed at relative humidity $\geq$ 25% of the aerosol sample flow. A consistent spot sample with a diameter of $D_{90} = 1.4$ mm (the diameter of a circle containing 90% of the deposited particles) was obtained regardless of the aerosol particle diameter ($d_p = 20$–1900 nm). For fiber counting applications using phase contrast microscopy, the TCAC can reduce the sampling time, or counting uncertainty, by two to three orders of magnitude, compared to the 25-mm-filter collection. The study shows that the proposed mixing-flow scheme enables a compact spot sample collector suitable for handheld or portable applications, while still allowing for high flow rates.

GRAPHICAL ABSTRACT

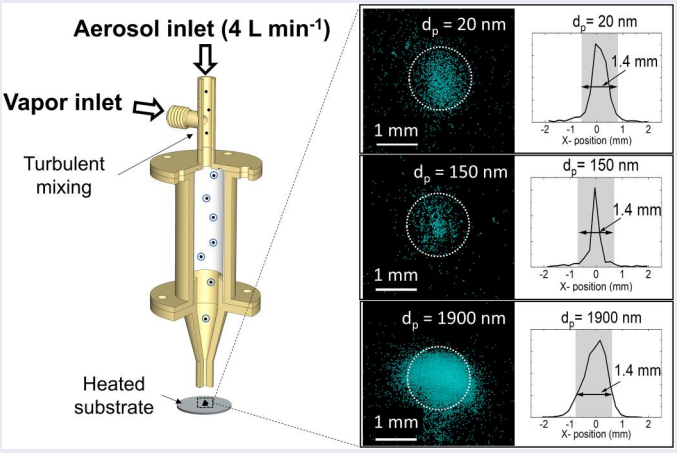

ARTICLE HISTORY
Received 4 December 2023
Accepted 17 May 2024

EDITOR
Coty Jen

1. Introduction

Aerosol chemical analysis often involves sample collection on particulate filter media followed by laboratory chemical analysis (Raynor et al. 2011). For aerosol exposure measurements, particularly involving personal sampling, 1–2 L min^{-1} sampling flow rates are customary and most standard methods recommend 2 L min^{-1} (NIOSH 1994a, 1994b, 2003; OSHA 2022). Despite the

CONTACT Pramod Kulkarni PSKulkarni@cdc.gov Centers for Disease Control and Prevention, National Institute for Occupational Safety and Health, Cincinnati, OH 45213, USA.

Supplemental data for this article is available online at https://doi.org/10.1080/02786826.2024.2361050

cost-effectiveness of the filter-based collection technique, sample collection on filter media does not allow real-time monitoring of aerosols. Sample redeposition from the filter media to different substrates or extraction into solvents is often required for various laboratory analytical and microscopy methods. Such redeposition, resuspension, or sample pretreatment can introduce matrix effects, sample damage, or even cause loss of target analytes. Furthermore, chemical analysis of a particulate filter media is often time-consuming, and analysis of the entire filter may not be practical using microscopy or laser or optical spectroscopy (Wei et al. 2017, 2020, 2022; Zervaki, Dionysiou, and Kulkarni 2023; Zheng et al. 2017, 2018).

To address some of these limitations, alternate methods have been developed to collect aerosol samples in a dry spot (Eiguren Fernandez, Lewis, and Hering 2014; Tajima et al. 2019; Zervaki et al. 2023) or in a liquid suspension (Jang, Bhardwaj, and Jang 2022; Lednicky et al. 2016; Pan, Lednicky, and Wu 2019; Pan et al. 2016). These techniques rely on the growth of particles into droplets *via* condensation in a laminar flow that is saturated with water vapor within a wet-walled tube. However, they either use smaller flow rates, typically below 1.5 L min^{-1} or achieve high sample throughputs with a substantial increase of the size of the collector.

Another commonly used method for condensation droplet growth is rapid adiabatic mixing of hot saturated vapor flow with cold aerosol-laden flow (Fuchs and Sutugin 1965; Okuyama, Kousaka, and Motouchi 1984; Parsons and Mavliev 2001; Yoshida, Kousaka, and Okuyama 1976). This method is usually referred to as "turbulent mixing". The mixing flow-type Condensation Nuclei Counters (CNCs), generate supersaturation due to the high vapor partial pressure of the mixture, eliminating the need for cooling. One of the advantages of this technique is the ability to implement higher aerosol flow rates compared to the laminar flow-type systems (Mavliev 2002; Parsons and Mavliev 2001) and minimize diffusional losses (Kim, Okuyama, and Shimada 2002).

This study involved the design and characterization of a new, compact, water-based, condensation droplet growth concentrator, the Turbulent-mixing, Condensation Aerosol Concentrator (TCAC) for spot sample collection, that operates at a relatively high aerosol sample flow rate at 4 L min^{-1}. We evaluated the effect of five variables on the operation of the concentrator: (1) the mixing ratio, defined as the vapor-to-aerosol flow rate ratio, (2) the particle diameter, (3) the saturator temperature, (4) the relative humidity of the inlet aerosol sample, and (5) the aerosol number concentration. An optimum set of operating parameters for acceptable performance was determined. Characteristics of the collected dry spot samples, such as spot diameter, and spatial distribution of particles were also investigated.

2. Materials and methods

2.1. Description of the TCAC

Figure 1a shows the configuration of the prototype TCAC system. The compact TCAC system device consists of four main components: a *saturator*, which generates hot water vapor-saturated flow; a *mixing section* where the hot saturated flow mixes with the cold aerosol flow, inducing supersaturation, seed activation, and droplet growth; a *growth tube*, which promotes further activation and droplet growth, and a *converging nozzle*, which concentrates the droplets into a focused beam for collection. The prototype unit has a volume of ~541 cm^3. Figure 1b shows the cross-sectional view of the mixing section, the growth tube, and the converging nozzle, where the activation, growth, and focusing of the droplets occur, respectively.

The *saturator* is a small reservoir ($43 \times 43 \times 25$ mm) with an approximate capacity of 45 ml of ultra-filtered distilled water. An immersion temperature sensor (model RTD-NPT-72-E; Omega Engineering Inc, Norwalk, CT, USA) is affixed on top of the saturator while the bottom houses an immersion water cartridge heater (Yancheng Xinrong Electronics Industry, Ltd., China). Both the temperature sensor and the immersion heater are connected to a temperature controller (model CN4116-R1-R2-LV; Omega Engineering Inc, Norwalk, CT, USA). Inside the saturator, there is a coiled tube made of Nafion™ (product TT-110; Perma Pure LLC, Lakewood, NJ, USA), a proton exchange membrane. Particle-free air at room temperature enters the Nafion™ tube and saturated hot air exits from the outlet. Based on finite element modeling (using Comsol™ Multiphysics, version 6.1) of the flow field and the heat and mass transfer within the Nafion™ tube, a 2-mm-ID and 30 cm long coiled tube was sufficient to generate a vapor-saturated flow (Section S1 in SI).

The *mixing section* of the TCAC consists of a "tee", where the cold particle-laden flow enters from the 4.2-mm-diameter top inlet, minimizing particle losses within the mixing zone, at a constant flow rate of 4 L min^{-1}. Simultaneously, the hot saturated flow, free of

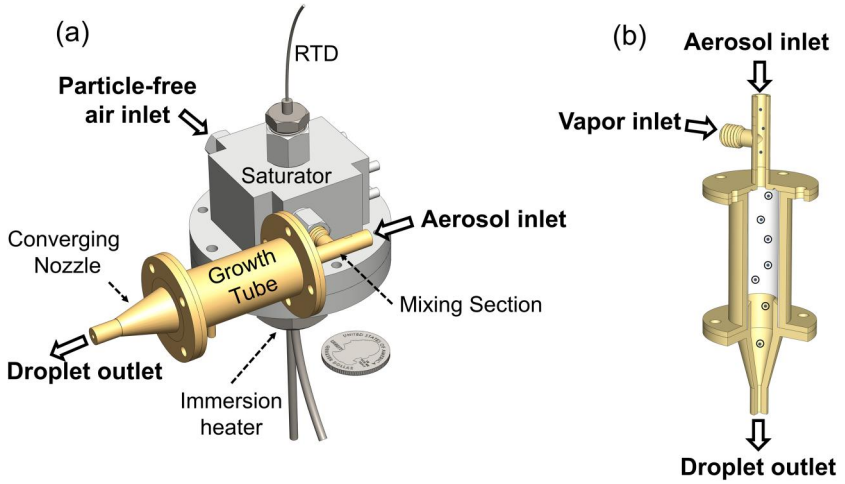

Figure 1. 3D view of (a) the overall assembly of TCAC and (b) the cross-sectional view of mixing, growth, and converging nozzle sections of the TCAC.

particles, enters at a 90° angle from a 4-mm-diameter side inlet, at a fixed flow rate ranging from 0.2 to 1.6 L min^{-1}. The hot saturated flow at a 90° angle impinges onto the large volume of aerosol flow, facilitating rapid mixing (Holunga, Flagan, and Atwater 2005). The two flows undergo rapid, turbulent mixing just downstream of the mixing zone, which leads to the supersaturation of water vapor in the mixed flow. A heat-resistant glass-filled resin was selected as the material for the mixing "tee" part through iterative experimentation. The volume of the mixing region where the turbulent mixing occurs is estimated to be 0.236 cm^3 and the residence time of the aerosols in this mixing region, assuming a fully developed flow, was estimated to be in the range of 2.5–3 ms.

Downstream of the mixing region, the mixed flow enters a 16-mm-ID *growth tube*. The length of the growth tube was 50 mm. Within the growth tube, the reduced flow velocity and increased residence time promote the activation and growth of almost all particles in the sample flow. The estimated residence time of the mixture inside the growth tube was at least 108 ms. The interior wall of the growth tube was covered with a lining made of porous glass fiber filter paper to allow the absorption of wall condensate. A peristaltic pump was used to rapidly remove the condensate from the filter liner to prevent water accumulation inside the growth tube.

A *converging nozzle* is used downstream of the *growth tube* to focus the grown droplets into a confined beam. The concentration of the droplets closer to the central axis for spot sample collection is crucial for enhanced analytical sensitivity and reduced detection limits. The length and the diameter of the converging nozzle were 20 and 1.7 mm, respectively. The particle diameter that can be collected with 50% efficiency, d_{p50}, was given by (Hinds and Zhu 2022; Marple and Olson 2011):

$$d_{p50}\sqrt{C_c} = \left(\frac{9\mu D_j Stk_{50}}{\rho_p U}\right)^{1/2} \quad (1)$$

where C_c is the Cunningham slip correction factor, μ is the dynamic viscosity of air, D_j is the nozzle jet diameter, Stk_{50} is the Stokes number corresponding to 50% collection efficiency (0.24 for round jet nozzles), ρ_p is the particle density, and U is the jet velocity. A flow rate of 4 L min^{-1} (without considering the hot saturated flow) guarantees the collection of droplets with an aerodynamic diameter of ~1.35 μm or larger.

2.2. Saturation ratio, Kelvin diameter, and droplet growth calculation

Calculations were performed to estimate the saturation ratio and Kelvin diameter. Ideal turbulent adiabatic mixing was assumed. Using the mass and enthalpy balance for the water vapor on a dry air basis, as well as adiabatic mixing of the two flows, the water vapor content and temperature of the mixed flow was given by:

$$H_m = \frac{Q_h H_h + Q_c H_c}{Q_h + Q_c} \quad (2)$$

$$T_m = \frac{C_h T_h Q_h + C_c T_c Q_c}{C_h Q_h + C_c Q_c} \quad (3)$$

where water vapor content is denoted by H, flow rate by Q (L min^{-1}), temperature by T (K), and specific heat capacity of air containing water vapor by C (cal $g_{dry,air}^{-1}$ K^{-1}). The subscripts h, c, and m refer to the hot, cold, and mixed flow, respectively. The water

vapor mass content and the specific heat capacity of air containing water vapor for a given stream "i" were calculated as follows (Okuyama, Kousaka, and Motouchi 1984):

$$H_i = \left(\frac{MW}{MW_a}\right)\left(\frac{P_i\ [mm\ Hg]}{760 - P_i\ [mm\ Hg]}\right) \tag{4}$$

$$C_i = C_{p,w}\ H_i + 0.24\ \left[cal\ g_{dry,air}{}^{-1}K^{-1}\right] \tag{5}$$

where MW is the molecular weight of water (18.02 g mol^{-1}), MW_a is the molecular weight of air (28.97 g mol^{-1}), P is the partial pressure of water vapor (mm Hg) and $C_{p,w}$ is the specific heat capacity of water vapor (0.47 cal g^{-1} K^{-1}).

Kelvin diameter (D_p*)—the threshold diameter of the particle that neither grows nor evaporates—was estimated using the following equation (Hinds and Zhu 2022; Seinfeld and Pandis 2012):

$$D_p{}^* = \frac{4\sigma MW}{\rho RT \ln S} \tag{6}$$

where σ and ρ are the surface tension and the density of the water droplet, respectively, R is the universal gas constant, and S (> 1) is the saturation ratio.

The droplet growth as a function of time (dD_p/dt) was given by Seinfeld and Pandis (2012):

$$D_p\frac{dD_p}{dt} = \frac{S\text{-}\exp(4\sigma MW/\rho RTD_p)}{(\rho RT/4P_0D'_vMW) + (\Delta H_v\rho/4k'_aT)((\Delta H_vMW/RT) - 1)} \tag{7}$$

where D_p is the droplet diameter, P_0 is the equilibrium vapor pressure, and ΔH_v is the specific latent heat of evaporation. The effective diffusivity of water vapor, D'_v, and thermal conductivity of air, k'_a, are given by Seinfeld and Pandis (2012):

$$D'_v = \frac{D_v}{\left(1 + (2D_v/a_cD_p)(2\pi MW/RT)^{1/2}\right)} \tag{8}$$

$$k'_a = \frac{k_a}{\left(1 + \left(2k_a/a_TD_p\rho_aC_{p,a}\right)(2\pi MW_a/RT)^{1/2}\right)} \tag{9}$$

where the diffusivity of the water is denoted by D_v, the mass and thermal accommodation coefficients are denoted by a_c and a_T, and the density, the molecular weight, and the heat capacity of air are denoted by ρ_a, MW_a, and $C_{p,a}$, respectively. The values or expressions of the parameters presented above are listed in Table S-1 in SI.

For simplicity, the latent heat released from the vapor condensation, or the vapor depletion was not accounted for. Both of these factors can result in a slight reduction of the saturation ratio or an increase in the Kelvin diameter, particularly at high particle number concentrations (Khlystov 1995; Lathem and Nenes 2011; Lewis and Hering 2013).

S and D_p* were calculated for the mixing of the cold aerosol flow ($T_c = 20\,^\circ$C) with the hot saturated flow ($T_h = 70$–$85\,^\circ$C) in the TCAC (Figures S-2 and S-3 in SI). The results indicate that a higher temperature of the hot flow (T_h) leads to a higher S (or smaller D_p*) peak. A smaller mixing ratio is required for a higher T_h. Furthermore, we calculated S for various ambient temperatures ($T_c = 0$, 10, 30, and 40 °C) at select hot saturated flow temperatures (Figure S-4 in SI). Turbulent mixing collectors can be sensitive to inlet sample flow temperature; higher ambient temperatures necessitate higher temperatures of the saturated flow. To reduce sensitivity to ambient temperatures, a temperature-conditioning stage could be added at the inlet to keep the sample flow temperature within the acceptable range.

We calculated the required time for droplet growth for saturator temperatures of 75, 80, and 85 °C, and at peak saturation ratios obtained for fixed mixing ratios (see Figure S-2 in SI). Droplets can grow to diameters $> 1.5\,\mu$m in ~2.5 ms—minimum residence time of the aerosols in the mixing region—assuming ideal mixing of the two flows, and constant temperature and vapor partial pressure (Figure S-5 in SI). Turbulent mixing can significantly reduce the required droplet growth time compared to the laminar flow-type condensation nuclei counters (Wang et al. 2002). However, droplet growth may be limited to the residence time of the particle/droplet in the growth tube (Okuyama, Kousaka, and Motouchi 1984). In the prototype TCAC, supersaturation and nuclei activation are promoted by the rapid turbulent mixing of the two flows, which is further enhanced by the extended residence time of the mixed flow as it enters the growth tube.

2.3. Experimental setup

We measured the particle activation and droplet growth efficiency of the TCAC as a function of five parameters: (1) the mixing ratio (Q_h/Q_c), (2) the saturator temperature (T_h), (3) the relative humidity of the aerosol flow, (4) the particle diameter of the sampled aerosol (d_p), and (5) the number concentration of the sampled aerosol. The dry spot diameter and particle radial distribution were also determined by collecting particles on a substrate downstream of the concentrator. The optimum window of operating parameters was then identified.

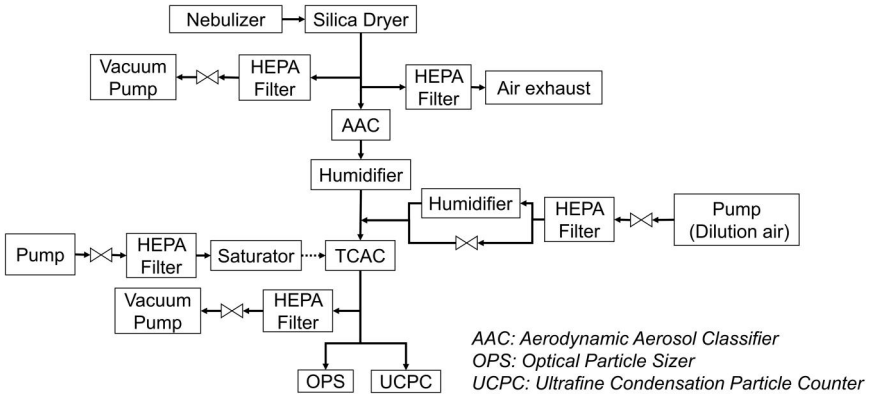

Figure 2. Experimental setup used for the growth efficiency measurements. Solid line arrow denotes flow of air stream. Dashed line arrow denotes flow of hot vapor-saturated stream.

Figure 2 shows the experimental setup used for characterizing the TCAC. A small-volume medical nebulizer (Salter 8900 Series; Salter Labs, Arvin, CA, USA) along with a diffusion dryer was used to generate sodium chloride test aerosol, at a flow rate of 3–4 L min^{-1}. An aerosol flow at atmospheric pressure was then introduced into the Aerodynamic Aerosol Classifier (AAC; Cambustion Ltd., Cambridge, UK) at a flow rate of 1.5 L min^{-1}, to generate a near-monodisperse test aerosol. Particle-free, dilution air was added downstream of the AAC to increase the total aerosol flow rate to 4 L min^{-1}, which was introduced into the TCAC. The humidity of the aerosol flow was varied using commercial Nafion^{TM} humidifiers (model MH-110-12F-4; Perma Pure LLC, Lakewood, NJ, USA) to control the relative humidity (*RH)* at 11, 15, 25, or 100%. No other *RH* conditions between 25 and 100% were explored due to similar growth efficiencies obtained under both conditions for saturator temperatures ≥75 °C. Particle-free flow was also introduced into the saturator of the TCAC to generate hot saturated flow. The saturator temperature was set to 70, 75, 80, or 85 °C, and the flow rate was set to 0.2, 0.4, 0.6, 0.8, 1.0, 1.2, 1.4, or 1.6 L min^{-1}. The flow rate of the hot saturated flow was measured at the inlet of the saturator at 22 °C. The flow rate across the TCAC was controlled within the range of 4.2–5.6 L min^{-1} by a vacuum pump and two particle counters: the Ultrafine Water-based Condensation Particle Counter (model 3786 UCPC; TSI Inc., Shoreview, MN, USA) and the Optical Particle Sizer (model 3330 OPS; TSI Inc., Shoreview, MN, USA).

The particle/droplet number concentration downstream of the TCAC was measured using the two particle counters. The UCPC provided a total number concentration of particles with a diameter in the range of 2.5 nm to > 3 µm, while the OPS classified particles into 16 different channels in the size range of 300 nm to 10 μm based on their optical diameter. The OPS was connected in parallel with the UCPC to detect and count the number of grown droplets and the final droplet optical diameter (d_d). The tubing transporting the aerosol from the TCAC outlet to the particle counters was thermally shielded using fiberglass woven tape to ensure that there was no change in the droplet size distribution. Moreover, the residence time of the particles/droplets in the TCAC growth tube was estimated to be > 0.1 s, providing sufficient time for activation and growth of all particles in the sample flow. Therefore, the droplets grew to collectable sizes before exiting the growth tube of the TCAC. The length of tubing from the outlet of the TCAC to the inlet of OPS and UCPC was kept identical to ensure similar transport losses.

In Section 2.1, we calculated the minimum collectable aerodynamic diameter (at which droplets could be collected by impaction), which was approximately ≥ 1.4 µm (d_p). Optical particle counters are typically calibrated with PSL spheres, which have a refractive index of 1.6. A pure water droplet has a refractive index of 1.33. As a result, water droplets are expected to appear undersized when detected by optical counters (Garvey and Pinnick 1983; Hinds and Kraske 1986; Pinnick, Garvey, and Duncan 1981). In this study, NaCl particles with an aerodynamic diameter (d_p) of ≥ 25 nm, were enlarged into droplets with d_d > 1400 nm. Assuming that the droplets were spherical, and made of pure water, the aerodynamic diameter was estimated to be 1.8 µm from Chien et al. (2016). However, the equation provided by Chien et al. (2016) was developed for oleic acid aerosol particles, which have a refractive index of 1.46, lower than that of PSL but larger than that of water. Therefore, the actual aerodynamic diameter of the water droplets is expected to be larger than 1.8 μm. As a result, the growth efficiency reported in this study, which accounted for both the nuclei activation and the droplet growth efficiency, was based on optical

diameters > 1.4 µm (unless stated otherwise), and was expressed as follows:

$$\eta = \frac{N_{1.4}}{N_T} \tag{10}$$

where η denotes the calculated growth efficiency, $N_{1.4}$ denotes the number concentration of droplets with $d_d > 1.4$ µm measured by the OPS, and N_T denotes the total number concentration of particles and/or droplets measured by the UCPC.

Wall losses within the TCAC were evaluated, in the absence of particle growth, by measuring the particulate mass, determined using gravimetric measurements, of the aerosol entering and exiting TCAC. Min-U-Sil@5 (US Silica, Katy, TX, USA) and Min-U-Sil@10 (IIT Research Institute, Chicago, IL, USA) were used as test particles. The aerosol sample flow was maintained at a flow rate of 4 L min^{-1} through the TCAC, while the saturated flow, entering from the side of the mixing "tee", had a flow rate of 0.6 L min^{-1}, all at room temperature to avoid particle growth. Downstream of the concentrator, a filter was positioned to capture the spot sample from the mixed flow exiting the TCAC and was subsequently used to determine the collected particulate mass. A parallel filter collection was performed to assess the particulate mass concentration of the aerosol entering the TCAC at identical conditions. The difference between the two particulate mass measurements was taken as the total wall loss within the TCAC system. No heating was applied at the saturator to prevent filter saturation and minimize pressure drop.

To measure the deposit diameter obtained using the TCAC, polystyrene nanospheres of 20 nm, 150 nm diameter (NIST Traceable Size Standards, Thermo Fisher Scientific, Waltham, MA, USA), and 1.9-µm-diameter fluorescent beads (fluoro-max green beads; Thermo Fisher Scientific, Waltham, MA, USA) were used as seed particles. The nano and microsphere aerosols were generated from liquid suspensions. The particles encapsulated within the grown droplets exiting the TCAC were collected on a flat heated surface at 90–100 °C ($T_{substrate}$) downstream of the TCAC, located at the experimentally determined optimum nozzle-to-plate distance of 4 mm. The droplets impacted directly onto an aluminum-backed, carbon tape (product 16086-5; Ted Pella Inc., Redding, CA, USA) that could be readily analyzed using Scanning Electron Microscopy (SEM; Phenom XL Desktop SEM, Thermo Fisher Scientific, Waltham, MA, USA) to obtain the dry spot diameter and the spatial distribution characteristics within the spot. The dry spot diameter, defined as the diameter of the circle encompassing 90% of the deposited particles, was calculated by determining the radial distribution of the projected area of the collected particles on the substrate, using the ImageJ software (Schneider, Rasband, and Eliceiri 2012). We expect negligible thermophoretic losses during droplet impaction, primarily due to the high velocity of the aerosol jet (> 30 m/s) and the very small thermal gradient to induce appreciable thermophoresis.

The number concentration of the test aerosol at the inlet of the concentrator was varied to investigate its impact on the performance of the TCAC. Dilution flow or make-up air was used to achieve the desired number concentrations. To minimize any effects on the performance of the concentrator due to the dilution, the mixing ratio was kept constant across the range of number concentrations tested.

3. Results and discussion

3.1. Optimum mixing ratio

Figure 3 shows the variation of the theoretically estimated saturation ratio of the mixed flow and experimentally measured growth efficiency of 25 nm sodium chloride seed particles (entering TCAC) as a function of the mixing ratio for four saturator temperatures. Regardless of the saturator temperature, the saturation ratio exceeded 1.0 after the mixing, indicating that particle activation and droplet growth were likely to occur. Figure 3a shows that when water vapor was generated at 70 °C and at a mixing ratio ranging from 0.15 to 0.25, approximately 60% of the particles grew to $d_d > 1.4\,\mu$m. Our findings suggest that the reduced efficiency was due to a decrease in the number of droplets that grew larger than 1.4 μm (d_d), rather than reduced activation of aerosol particles (see Figure S-6 in SI). We speculate that this may be attributed to both non-ideal adiabatic mixing as initially assumed, and to the generated heat during condensation, which may have caused the saturation ratio to drop significantly. However, we did not conduct further investigation into this matter, as it is beyond the scope of our work, and would require a different experimental design and instrumentation that is not available to us. Conversely, at saturator temperatures of 75, 80, and 85 °C, and at a mixing ratio of 0.2, 0.15, and 0.15, respectively, nearly all particles grew to $d_d > 1.4\,\mu$m (Figures 3b–d).

According to Figure 3, the peak saturation ratio was found to be proportional to T_h, with higher values observed at higher T_h. Generally, the minimum particle diameter that can be activated and the final droplet size attained depends on the saturation ratio, along

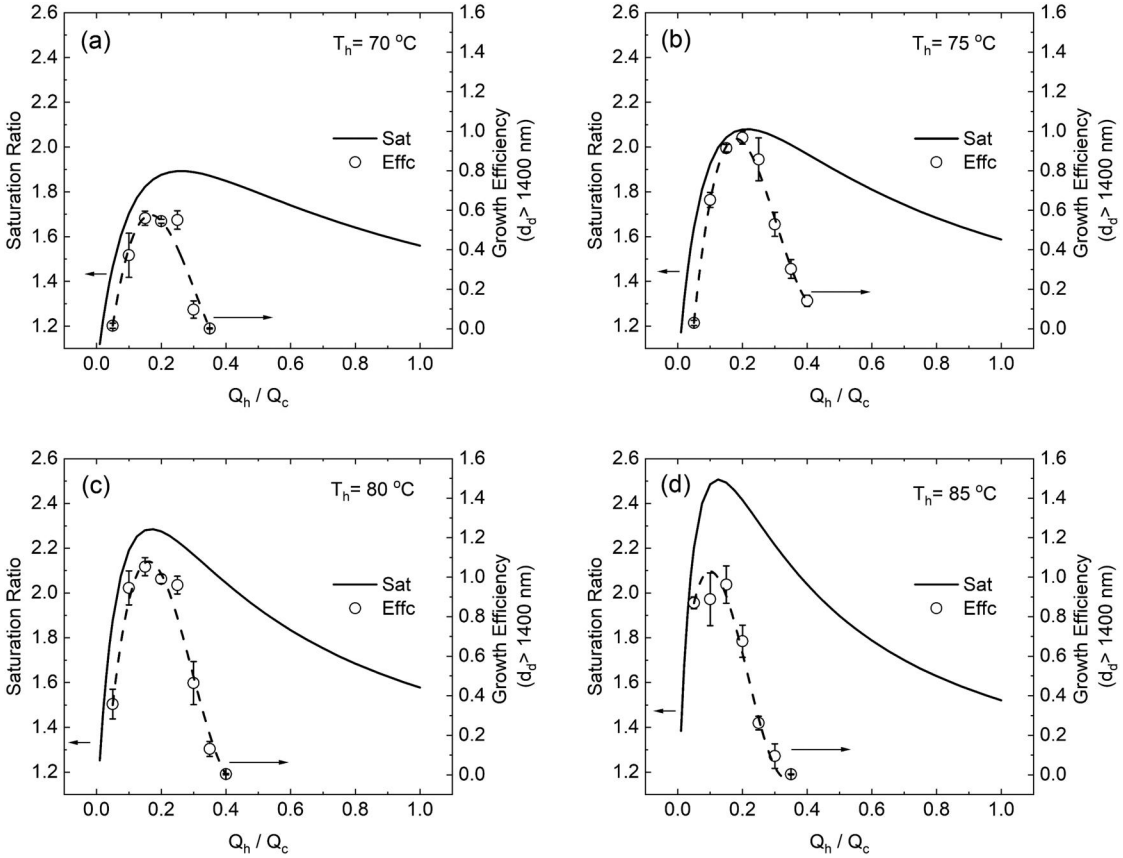

Figure 3. Calculated saturation ratio (Sat) compared to the experimental growth efficiency ($d_d > 1400$ nm; Effc) measured for 25 nm particles of NaCl, for a saturator temperature (T_h) of (a) 70 °C, (b) 75 °C, (c) 80 °C, and (d) 85 °C. The aerosol (cold) flow had a temperature of 22 °C and 100% humidity. The dashed line represents a fitted curve to the experimentally measured growth efficiency. The error bars indicate the standard deviation that was calculated from the three replicates.

with other parameters. The peaks of the calculated saturation ratio and the experimental growth efficiency were in good agreement, at specific T_h. However, the corresponding mixing ratio required to achieve the saturation and/or growth efficiency peak varied with T_h. When the hot flow temperature was 70 °C, the saturation ratio reached its maximum value at 1.89, corresponding to a mixing ratio of 0.25. In the experimental growth efficiency curve, a plateau was observed in the mixing ratio range of 0.15–0.25, which included the optimum mixing ratio value predicted theoretically. When the hot flow temperature was set to 75, 80, and 85 °C, the maximum saturation values calculated were 2.08, 2.28, and 2.51 at mixing ratios of 0.225, 0.175, and 0.125, respectively. Thus, for subsequent experiments, optimum mixing ratios were selected based on the hot flow temperature used, to ensure optimal performance of the concentrator.

3.2. Particle diameter

Figure 4 shows the growth efficiency as a function of the aerodynamic diameter of the seed particles, at different T_h values ranging from 70 to 85 °C. At 75, 80, and 85 °C the growth efficiency was > 86, 92, and 93%, respectively, for seed particles with aerodynamic diameters, d_p, ranging from 25 to 300 nm. The growth efficiency dropped to about 40–70% at $T_h = 70$ °C, indicating that a significant fraction of particles ($\sim$ 55%) did not grow beyond 1.4 μm. On the other hand, growth efficiency for $d_d > 300$ nm, was $\geq$ 90% (Figure S-6 in SI). Based on these results, a saturator temperature in the range of 75–85 °C was selected for the current study.

Figures S-7 and S-8 in SI show calculated transport efficiency and measured wall losses due to diffusion and inertial impaction in the TCAC. For nanoparticles with a d_p as small as 2 nm, negligible diffusive deposition is expected due to relatively high flow rates across the TCAC (Figure S-7 in SI; Kim, Okuyama, and Shimada 2002). Minimal inertial deposition losses ($\leq$ 10%) were measured experimentally inside the growth tube for d_p up to 10 μm (Figure S-8 in SI). When using the converging nozzle with an outlet diameter of 1.7 mm, the total wall losses were < 15% for $d_p \leq 5$ μm and < 20% for $d_p \leq 10$ μm.

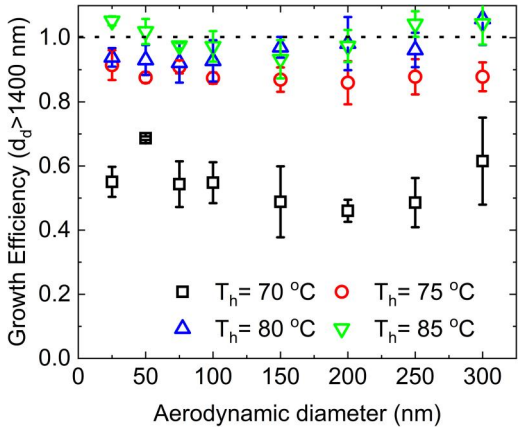

Figure 4. Growth efficiency ($d_d > 1400$ nm) measured as a function of the particle aerodynamic diameter when T_h was set to 70, 75, 80, and 85 °C. The temperature and inlet humidity of the aerosol (cold) flow was 22 °C and 100%, respectively. The error bars indicate the standard deviation that was calculated from the three replicates.

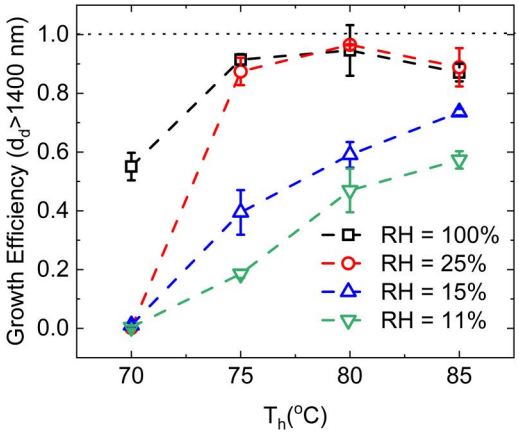

Figure 5. Growth efficiency ($d_d > 1400$ nm) measured as a function of T_h, for 25 nm NaCl particles and aerosol inlet humidity of 100, 25, 15, and 11%. The aerosol (cold) flow was at 22 °C. The error bars indicate the standard deviation of three repeat measurements.

3.3. Relative humidity

The performance of the TCAC was tested under various relative humidity conditions of the sampled aerosol flow (Figure 5). Figure 5 shows that the growth efficiency was ≥ 87% at saturator temperatures above 75 °C when the relative humidity of the sampled aerosol flow was between 25 and 100%. Based on these measurements, the recommended optimum inlet relative humidity range is 25–100% for $T_h \geq 75$ °C. To obtain higher growth efficiencies at lower inlet *RH* below 25%, T_h above 85 °C may be necessary.

Sodium chloride particles are prone to size changes depending on the surrounding relative humidity, due to deliquescence effects (Hämeri et al. 2001; Hering et al. 2005). An *RH* of ≥ 75% can lead to water absorption and an increase in particle diameter (Biskos et al. 2006; Cziczo and Abbatt 2000). However, NaCl and Ag aerosols are commonly used to characterize condensation particle counters (Cheng 2011; Kesten, Reineking, and Porstendörfer 1991; Scheibel and Porstendörfer 1983). The minimum activation particle diameter for a given CPC, obtained using NaCl and Ag aerosols can differ by a few nanometers (Romay et al. 2016). This difference is negligible considering that the TCAC was designed to be an aerosol sample collector for analytical applications. Moreover, the measured growth efficiency of 25-nm-diameter aerosol as a function of sample flow *RH* ranging from 25 to 100% was consistent for $T_h \geq 75$ °C, indicating minimal impact of deliquescence effects on the operational efficiency of the collector.

3.4. Performance stability

Complete growth at detectable droplet diameters ($d_d > 300$ nm) was observed for at least 60 min of continuous operation (Figure 6). Growth efficiency remained constant and was approximately close to 87% for the $d_d > 1400$ nm size fraction.

The mixing flow-type condensation growth technique relies on rapidly mixing a hot vapor stream with a cold aerosol-laden gas in an adiabatic process. The mixing chamber of the TCAC does not have active cooling, yet the desired temperature difference between the hot and cold flows was maintained during extended operation, indicating that the steady-state temperatures of the flows and mixing chamber walls were achieved quickly and that the performance of the system did not diminish with time due to inadequate thermal insulation.

3.5. Dry spot characteristics

Several tests were performed to determine the optimal nozzle-to-plate distance, which would result in a similar, small spot deposit for a wide range of PSL particle diameters. Large droplets are expected to converge closer to the nozzle exit compared to small droplets that converge further downstream. However, as the distance downstream increases, large droplets start diverging away from their focal point (Hari, McFarland, and Hassan 2007), as shown in Figure S-9 in the SI. We tested a range of nozzle-to-plate distance (denoted as *L*) from 4 to 10 mm, using PSL aerosol particles with $d_p = 1900$ nm. The aerosol flow rate was fixed at 4 L min^{-1}, the hot saturated flow rate at 0.8 L min^{-1}, and

the saturator temperature at 75 °C. The optimal nozzle-to-plate distance within the tested range was determined to be 4 mm.

Figures 7a–c show scanning electron micrographs of dry spots obtained for test PSL aerosol with $d_p = 20$, 150, and 1900 nm diameter. The calculated dry spot diameter, D_{90}, is shown in Figures 7d–f. The D_{90} of the spot sample was found to be independent of the seed particle diameter at the inlet of the TCAC and was ~1.4 mm for all PSL spheres tested. Additionally, the measured spot diameter was slightly smaller compared to the 1.7-mm converging nozzle diameter. The Full Width Half Maximum (FWHM) of a Gaussian distribution fitted to the axial distribution of deposited PSL particles was calculated to be 0.65, 0.29, and 1.01 mm for particle diameters of 20, 150, and 1900 nm, respectively. The reason for the sharper axial distribution of the 150 nm particles was not fully investigated. We speculate that this could be attributed to a more concentrated focusing of the droplets containing the 150 nm particles compared to the slightly greater spread of the droplets containing the 20 nm particles and the overfocused droplets containing the 1900 nm particles. Nevertheless, the deposit diameter remained consistent across all particle diameters. Figure S-10 in SI shows spot sample characteristics of 150 nm diameter PSL nanospheres at a saturator temperature of 80 and 85 °C. Similar deposition areas were observed, with a spot diameter of ~1.4 and 1.2 mm for 80 and 85 °C, respectively.

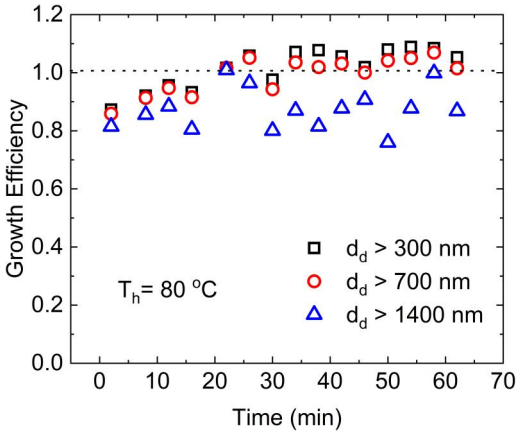

Figure 6. Growth efficiency measured based on three droplet size fractions ($d_d > 300$ nm, $d_d > 700$ nm, and $d_d > 1400$ nm), as a function of the operation time, for 25 nm NaCl particles. The aerosol (cold) flow had a temperature of 22 °C and 100% humidity. The saturator temperature (T_h) was 80 °C. A flow rate of 4 L min^{-1} was used for the aerosol (cold) flow and a flow rate of 0.6 L min^{-1} was used for the vapor-saturated (hot) flow.

3.6. Aerosol number concentration effect

Figure 8 shows the effect of particle number concentration on the growth efficiency of 25-nm-diameter NaCl seed particles. Growth efficiency remained high (> 85%) up to a number concentration of 3×10^4 cm^{-3}, beyond which the growth efficiency dropped slightly. This could possibly be due to vapor depletion or reduction in supersaturation due to heat released during the vapor condensation (Lewis and Hering 2013).

As the number concentration of sampled particles increases, the final droplet size decreases, and the threshold particle size that can be activated and grown into a droplet increases (Yoshida, Kousaka, and

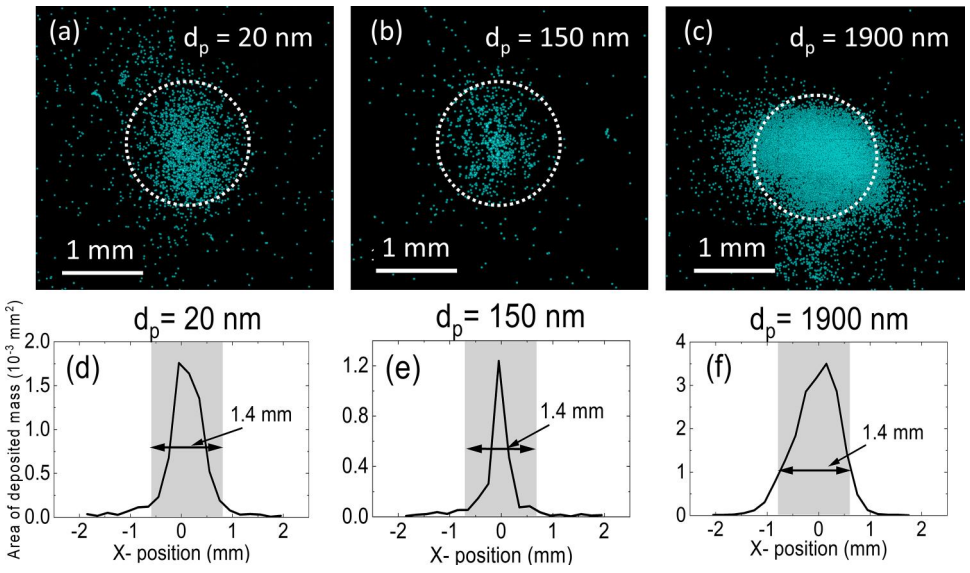

Figure 7. (a–c) SEM images and (d–f) axial distributions of deposited polystyrene spheres with $d_p = 20$, 150, and 1900 nm. The collection was attained at $T_h = 75$ °C, $Q_h = 0.8$ L min^{-1}, $Q_c = 4$ L min^{-1}, $T_c = 23$ °C, RH = 59–65%, and $T_{substrate} = 90$–100 °C.

Okuyama 1976). Okuyama, Kousaka, and Motouchi (1984) showed that the final droplet diameter depends on both the saturation ratio and the particle number concentration. They showed that the saturation ratio decreases more rapidly with increasing number concentration due to the heat release during vapor condensation. They concluded that at low number concentrations, droplet growth continues for a longer time, with the residence time being the primary limiting factor. In contrast, at higher particle number concentrations, droplet growth terminates much earlier, leading to a smaller or negligible effect of particle residence time on the final droplet size. According to Lewis and Hering (2013), in water-based laminar-flow type condensation growth systems, condensational heat release generally prevails over the vapor depletion effect, which often occurs at high particle number concentrations ($>10^6\,cm^{-3}$).

3.7. Counting uncertainty for fiber concentration measurement

The application of TCAC to the measurement of airborne fiber concentrations was investigated. Fiber counting using Phase Contrast Microscopy (PCM) is a common method for quantifying fiber concentration collected on a filter. The NIOSH method 7400 recommends collecting fibers on 25-mm filters for PCM analysis (NIOSH 2019); however, other collection techniques can also be used to concentrate the fiber sample in a small spot deposit, reducing counting uncertainty and sampling time. Shorter collection times are essential for rapid detection of airborne fibers, such as asbestos fibers, given their potential hazard even at low concentrations (NIOSH 2019). We estimated the sampling time required to achieve a targeted Poisson counting uncertainty for fiber concentration measurements using PCM for different collection methods: TCAC, Sequential Spot Sampler, and filter-based collection.

Sampling of a large number of fibers, n, can reduce the counting uncertainty ($\sigma\% = 1/\sqrt{n}$). For PCM analysis, the NIOSH method 7400 recommends a substrate area of $0.785\,mm^2$ (A_m), and a fiber density of $100–1300\,mm^{-2}$, for optimal and unbiased counting ($\sigma = 2.8–10\%$; NIOSH 2019). Assuming a fiber concentration of $0.1\,cm^{-3}$ (c_f), the required sampling time (t_c) to achieve a target counting uncertainty of 3–10% was calculated:

$$t_c = \frac{nA_d}{A_m c_f Q \eta_c} \tag{11}$$

where A_d is the spot deposit area of each collection technique, Q is the sample flow rate employed in each collection method, and η_c is the collection efficiency. The operating parameters of the aerosol collection methods used for the calculation of the required sampling time are listed in Table S-2 in SI. The spot sample generated from TCAC has an area of $\sim 1.54\,mm^2$, while the effective collection area of the Sequential Spot Sampler and the 25-mm filter are 0.785 and $385\,mm^2$, respectively.

The spot deposits generated by the TCAC, and the Sequential Spot Sampler can reduce the sampling time—for the same target counting uncertainty

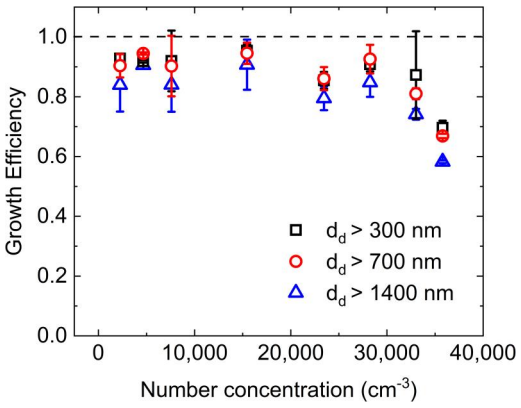

Figure 8. Growth efficiency ($d_d > 300$ nm, $d_d > 700$ nm, and $d_d > 1400$ nm) measured as a function of the particle number concentration for 25 nm NaCl particles. The temperature and inlet humidity of the aerosol (cold) flow was 22 °C and 100%, respectively. A flow rate of 4 L min^{-1} was used for the aerosol (cold) flow and a flow rate of 0.8 L min^{-1} was used for the vapor-saturated (hot) flow. The saturator temperature (T_h) was 75 °C.

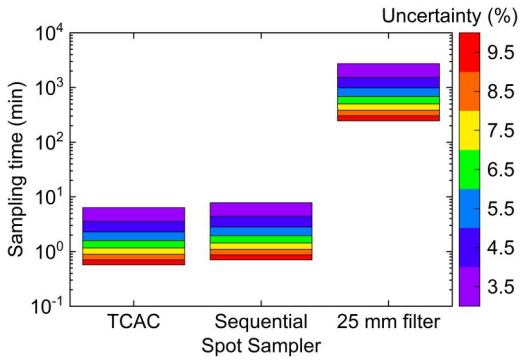

Figure 9. Comparison of estimated counting statistics for fiber concentration measurements using Phase Contrast Microscopy (PCM) analysis (NIOSH Method 7400) for different collection methods: TCAC, the Sequential Spot Sampler, and the filter-based collection. The Y-axis shows the sampling time required for attaining a target counting uncertainty (in the range of 3–10% as shown by graded color scale). The TCAC can significantly reduce sample collection time—or counting uncertainty—approximately by two to three orders of magnitude compared to the 25-nm filter collection.

($\sigma = 3$–10%)—approximately by two to three orders of magnitude compared to the 25-nm filter collection (Figure 9). Specifically, for a target counting uncertainty of 3%, the TCAC and the Sequential Spot Sampler would require only 6 and 8 min of fiber sampling, respectively, while the 25-nm filter collection would require 2725 min.

4. Conclusions

A new water-based condensation aerosol concentrator, called the Turbulent-mixing, Condensation Aerosol Concentrator (TCAC), was developed to obtain dry spot samples at aerosol flow rates up to 4 L min^{-1}. The optimum operating configuration was identified for an ambient aerosol temperature at ~20 °C. Lower mixing flow rate ratios were required for higher temperatures of the hot saturated flow (T_h). Particles with $d_p \geq 25$ nm could be grown to droplets with $d_d > 1400$ nm with nearly 100% efficiency when $T_h \geq 75$ °C and the cold aerosol flow was at room temperature. The TCAC could achieve high growth efficiency with a minimum *RH* of 25% of the particle-laden airflow. The device could collect aerosols on a small spot on a substrate *via* impaction ($D_{90} = 1.4$ mm) for a wide range of seed particle diameters ($d_p = 20$–1900 nm). In addition, for fiber counting applications using phase contrast microscopy, the TCAC can significantly reduce sample collection time—or counting uncertainty—compared to the 25-mm filter collection, by two to three orders of magnitude. The ability of the TCAC to activate and collect particles with various diameters, its compact size, and high sample flow rates make it a good alternative. The compact, high flow rate, water-based, mixing flow condensation scheme can be used in a small, hand-held, portable instrument for the collection and subsequent analysis of nano- and micro-particles using microscopy or laser spectroscopic methods, such as Raman, reflectance, absorption, fluorescence, or emission spectroscopy.

Acknowledgments

The authors would like to thank Dr. Kabir Rishi and Dr. Bon-Ki Ku for their valuable feedback on this manuscript.

Disclosure statement

No potential conflict of interest was reported by the author(s).

Disclaimer

The findings and conclusions in this report are those of the author(s) and do not necessarily represent the official position of the National Institute for Occupational Safety and Health, Centers for Disease Control and Prevention.

Funding

This research was supported by a NIOSH intramural NORA grant.

ORCID

Orthodoxia Zervaki http://orcid.org/0000-0002-3481-506X
Dionysios D. Dionysiou http://orcid.org/0000-0002-6974-9197
Pramod Kulkarni http://orcid.org/0000-0001-7692-4662

References

Biskos, G., A. Malinowski, L. M. Russell, P. R. Buseck, and S. T. Martin. 2006. Nanosize effect on the deliquescence and the efflorescence of sodium chloride particles. *Aerosol Sci. Technol.* 40 (2):97–106. doi: 10.1080/02786820500484396.

Cheng, Y.-S. 2011. Condensation particle counters. In *Aerosol measurements: Principles, techniques and applications*, ed. P. Kulkarni, P. A. Baron, and K. Willeke, 381–92. 3rd ed. Hoboken, NJ: Wiley. doi: 10.1002/9781118001684.

Chien, C. H., A. Theodore, C. Y. Wu, Y. M. Hsu, and B. Birky. 2016. Upon correlating diameters measured by optical particle counters and aerodynamic particle sizers. *J. Aerosol Sci.* 101:77–85. doi: 10.1016/j.jaerosci.2016.05.011.

Cziczo, D. J., and J. P. D. Abbatt. 2000. Infrared observations of the response of NaCl, $MgCl_2$, NH_4 HSO_4, and NH_4NO_3 aerosols to changes in relative humidity from 298 to 238 K. *J. Phys. Chem. A* 104 (10):2038–47. doi: 10.1021/jp9931408.

Eiguren Fernandez, A., G. S. Lewis, and S. V. Hering. 2014. Design and laboratory evaluation of a sequential spot sampler for time-resolved measurement of airborne particle composition. *Aerosol Sci. Technol.* 48 (6):655–63. doi: 10.1080/02786826.2014.911409.

Fuchs, N. A., and A. G. Sutugin. 1965. Coagulation rate of highly dispersed aerosols. *J. Colloid Sci.* 20 (6):492–500. doi: 10.1016/0095-8522(65)90031-0.

Garvey, D. M., and R. G. Pinnick. 1983. Response characteristics of the particle measuring systems active scattering aerosol spectrometer probe (ASASP–X). *Aerosol Sci. Technol.* 2 (4):477–88. doi: 10.1080/02786828308958651.

Hämeri, K., A. Laaksonen, M. Väkevä, and T. Suni. 2001. Hygroscopic growth of ultrafine sodium chloride particles. *J. Geophys. Res.* 106 (D18):20749–57. doi: 10.1029/2000JD000200.

Hari, S., A. R. McFarland, and Y. A. Hassan. 2007. CFD study on the effects of the large particle crossing trajectory phenomenon on virtual impactor performance.

Aerosol Sci. Technol. 41 (11):1040–8. doi: 10.1080/02786820701697549.

Hering, S. V., M. R. Stolzenburg, F. R. Quant, D. R. Oberreit, and P. B. Keady. 2005. A laminar-flow, water-based condensation particle counter (WCPC). *Aerosol Sci. Technol.* 39 (7):659–72. doi: 10.1080/02786820500182123.

Hinds, W. C., and G. Kraske. 1986. Performance of PMS model LAS-X optical particle counter. *J. Aerosol Sci.* 17 (1):67–72. doi: 10.1016/0021-8502(86)90007-8.

Hinds, W. C., and Y. Zhu. 2022. *Aerosol technology: Properties, behavior, and measurement of airborne particles*. 3rd ed. Hoboken, NJ: Wiley.

Holunga, D. M., R. C. Flagan, and H. A. Atwater. 2005. A scalable turbulent mixing aerosol reactor for oxide-coated silicon nanoparticles. *Ind. Eng. Chem. Res.* 44 (16):6332–41. doi: 10.1021/ie049172l.

Jang, J., J. Bhardwaj, and J. Jang. 2022. Efficient measurement of airborne viable viruses using the growth-based virus aerosol concentrator with high flow velocities. *J. Hazard. Mater.* 434 (July):128873. doi: 10.1016/j.jhazmat.2022.128873.

Kesten, J., A. Reineking, and J. Porstendörfer. 1991. Calibration of a TSI model 3025 ultrafine condensation particle counter. *Aerosol Sci. Technol.* 15 (2):107–11. doi: 10.1080/02786829108959517.

Khlystov, A. 1995. The steam-jet aerosol collector. *Atmos. Environ.* 29 (17):2229–34. doi: 10.1016/1352-2310(95)00180-7.

Kim, C. S., K. Okuyama, and M. Shimada. 2002. Performance of a mixing-type CNC for nanoparticles at low-pressure conditions. *J. Aerosol Sci.* 33 (10):1389–404. doi: 10.1016/S0021-8502(02)00092-7.

Lathem, T. L., and A. Nenes. 2011. Water vapor depletion in the DMT continuous-flow CCN chamber: Effects on supersaturation and droplet growth. *Aerosol Sci. Technol.* 45 (5):604–15. doi: 10.1080/02786826.2010.551146.

Lednicky, J., M. Pan, J. Loeb, H. Hsieh, A. Eiguren-Fernandez, S. Hering, Z. H. Fan, and C.-Y. Wu. 2016. Highly efficient collection of infectious pandemic influenza H1N1 virus (2009) through laminar-flow water based condensation. *Aerosol Sci. Technol.* 50 (7):i–iv. doi: 10.1080/02786826.2016.1179254.

Lewis, G. S., and S. V. Hering. 2013. Minimizing concentration effects in water-based, laminar-flow condensation particle counters. *Aerosol Sci. Technol.* 47 (6):645–54. doi: 10.1080/02786826.2013.779629.

Marple, V. A., and B. A. Olson. 2011. Sampling and measurement using inertial, gravitational, centrifugal, and thermal techniques. In *Aerosol measurement: Principles, techniques, and applications*, ed. Pramod Kulkarni, Paul A. Baron, and Klaus Willeke, 129–52. 3rd ed. Hoboken, NJ: Wiley.

Mavliev, R. 2002. Turbulent mixing condensation nucleus counter. *Atmos. Res.* 62 (3–4):303–14. doi: 10.1016/S0169-8095(02)00016-9.

NIOSH. 1994a. Particulates not otherwise regulated, total: Method 0500. In *NIOSH manual of analytical methods (NMAM)*. 4th ed. https://www.cdc.gov/niosh/docs/2003-154/pdfs/0500.pdf.

NIOSH. 1994b. Carbon black: Method 5000. In *NIOSH manual of analytical methods (NMAM)*. 4th ed. https://www.cdc.gov/niosh/docs/2003-154/pdfs/5000.pdf.

NIOSH. 2003. Silica, crystalline, by XRD (filter redeposition): Method 7500. In *NIOSH manual of analytical methods (NMAM)*. 4th ed. https://www.cdc.gov/niosh/docs/2003-154/pdfs/7500.pdf.

NIOSH. 2019. Asbestos and other fibers by PCM: Method 7400. In *NIOSH manual of analytical methods (NMAM)*. 5th ed. https://www.cdc.gov/niosh/nmam/pdf/7400.pdf.

Okuyama, K., Y. Kousaka, and T. Motouchi. 1984. Condensational growth of ultrafine aerosol particles in a new particle size magnifier. *Aerosol Sci. Technol.* 3 (4):353–66. doi: 10.1080/02786828408959024.

OSHA. 2022. 29 CFR Part 1910.1001 occupational exposure to asbestos. https://www.govinfo.gov/content/pkg/CFR-2022-title29-vol6/pdf/CFR-2022-title29-vol6-sec1910-1001.pdf.

Pan, M., A. Eiguren-Fernandez, H. Hsieh, N. Afshar-Mohajer, S. V. Hering, J. Lednicky, Z. Hugh Fan, and C. -Y. Wu. 2016. Efficient collection of viable virus aerosol through laminar-flow, water-based condensational particle growth. *J. Appl. Microbiol.* 120 (3):805–15. doi: 10.1111/jam.13051.

Pan, M., J. A. Lednicky, and C. -Y. Wu. 2019. Collection, particle sizing and detection of airborne viruses. *J. Appl. Microbiol.* 127 (6):1596–611. doi: 10.1111/jam.14278.

Parsons, C., and R. Mavliev. 2001. Design and characterization of a new, water-based, high sample-flow condensation nucleus counter. *Aerosol Sci. Technol.* 34 (4):309–20. doi: 10.1080/02786820117366.

Pinnick, R. G., D. M. Garvey, and L. D. Duncan. 1981. Calibration of Knollenberg FSSP light-scattering counters for measurement of cloud droplets. *J. Appl. Meteor.* 20 (9):1049–57. doi: 10.1175/1520-0450(1981)020<1049:COKFLS>2.0.CO;2.

Raynor, P. C., D. Leith, K. W. Lee, and R. Mukund. 2011. Sampling and analysis using filters. In *Aerosol measurement*, ed. Pramod Kulkarni, Paul A. Baron, and Klaus Willeke, 107–28. 3rd ed. Hoboken, NJ: Wiley. doi: 10.1002/9781118001684.ch7.

Romay, F. J., A. M. Collins, W. D. Dick, L. Li, C. W. Fandrey, and B. Y. H. Liu. 2016. Water-based single-flow mixing condensation particle counter. *Aerosol Sci. Technol.* 50 (12):1320–6. doi: 10.1080/02786826.2016.1222510.

Scheibel, H. G., and J. Porstendörfer. 1983. Generation of monodisperse Ag- and NaCl-aerosols with particle diameters between 2 and 300 Nm. *J. Aerosol Sci.* 14 (2):113–26. doi: 10.1016/0021-8502(83)90035-6.

Schneider, C. A., W. S. Rasband, and K. W. Eliceiri. 2012. NIH image to ImageJ: 25 Years of image analysis. *Nat. Methods* 9 (7):671–5. doi: 10.1038/nmeth.2089.

Seinfeld, J. H., and S. N. Pandis. 2012. Cloud physics. In *Atmospheric chemistry and physics: From air pollution to climate change*, 1333. 2nd ed. Hoboken, NJ: Wiley.

Tajima, N., K. Iida, K. Ehara, S. Khumpuang, S. Hara, and H. Sakurai. 2019. A method to deposit a known number of polystyrene latex particles on a flat surface. *Aerosol Sci. Technol.* 53 (12):1353–66. doi: 10.1080/02786826.2019.1666969.

Wang, J., V. F. McNeill, D. R. Collins, and R. C. Flagan. 2002. Fast mixing condensation nucleus counter: Application to rapid scanning differential mobility

analyzer measurements. *Aerosol Sci. Technol.* 36 (6):678–89. doi: 10.1080/02786820290038366.

Wei, S., B. Johnson, M. Breitenstein, L. Zheng, J. Snawder, and P. Kulkarni. 2022. Aerosol analysis using handheld Raman spectrometer: On-site quantification of trace crystalline silica in workplace atmospheres. *Ann. Work Expo. Health* 66 (5):656–70. doi: 10.1093/annweh/wxab076.

Wei, S., P. Kulkarni, K. Ashley, and L. Zheng. 2017. Measurement of crystalline silica aerosol using quantum cascade laser–based infrared spectroscopy. *Sci. Rep.* 7 (1): 13860. doi: 10.1038/s41598-017-14363-3.

Wei, S., P. Kulkarni, L. Zheng, and K. Ashley. 2020. Aerosol analysis using quantum cascade laser infrared spectroscopy: Application to crystalline silica measurement. *J. Aerosol Sci.* 150 (December):105643. doi: 10.1016/j.jaerosci.2020.105643.

Yoshida, T., Y. Kousaka, and K. Okuyama. 1976. Growth of aerosol particles by condensation. *Ind. Eng. Chem. Fund.* 15 (1):37–41. doi: 10.1021/i160057a007.

Zervaki, O., D. D. Dionysiou, and P. Kulkarni. 2023. Characterization of a multi-stage focusing nozzle for collection of spot samples for aerosol chemical analysis. *J. Aerosol Sci.* 174 (November):106235. doi: 10.1016/j.jaerosci.2023.106235.

Zervaki, O., B. Stump, P. Keady, D. D. Dionysiou, and P. Kulkarni. 2023. NanoSpot^{TM} collector for aerosol sample collection for direct microscopy and spectroscopy analysis. *Aerosol Sci. Technol.* 57 (4):342–54. doi: 10.1080/02786826.2023.2167648.

Zheng, L., P. Kulkarni, M. E. Birch, K. Ashley, and S. Wei. 2018. Analysis of crystalline silica aerosol using portable Raman spectrometry: Feasibility of near real-time measurement. *Anal. Chem.* 90 (10):6229–39. doi: 10.1021/acs.analchem.8b00830.

Zheng, L., P. Kulkarni, K. Zavvos, H. Liang, M. E. Birch, and D. D. Dionysiou. 2017. Characterization of an aerosol microconcentrator for analysis using microscale optical spectroscopies. *J. Aerosol Sci.* 104 (February):66–78. doi: 10.1016/j.jaerosci.2016.11.007.